

**Transversely isotropic elastic properties of multiwalled carbon nanotubes**

Lianxi Shen and Jackie Li\*

*Mechanical Engineering Department, City College of New York, City University of New York, 140th and Convent Avenue, New York, New York 10031, USA*

(Received 31 March 2004; revised manuscript received 11 August 2004; published 19 January 2005)

Five independent effective elastic moduli of a transversely isotropic multiwalled carbon nanotube (MWNT) are studied by analyzing its deformations under four loading conditions, i.e., axial tension, torsional moment, in-plane biaxial tension, and in-plane tension-compression stress. Two distributions of the tension loading on the outermost tube and on all tubes are considered, which correspond to the tensile and compressive Young's moduli. The general relations between the interwall stresses and strains are linearized due to the small strain condition, where the interwall stresses correspond to the variation of the interwall van der Waals forces. Three interwall elastic constants are used to characterize the linear relations associated with three basic interwall deformation modes, i.e., normal deformation in radial direction and two shear deformations in axial and circumferential directions. By taking each tube as a single-walled carbon nanotube, the analytical expressions for the interwall shear stress under the tensile loading on the outermost tube and five elastic moduli of a double-walled carbon nanotube are first obtained. Then, a replacement method is proposed to derive the corresponding expressions for the cases of more walls than two. These analytical expressions are plotted for the case of MWNT's composed of armchair tubes, where the interwall elastic constants are approximated as the corresponding ones of the graphite. The effect of the wall number, diameter, chirality, and length of the MWNT on the shear stress and five elastic moduli are displayed and discussed.

DOI: 10.1103/PhysRevB.71.035412

PACS number(s): 62.25.+g, 62.20.Dc, 68.35.Gy, 61.46.+w

**I. INTRODUCTION**

Experiments and theoretical predictions have shown that carbon nanotubes (CNT's) can possess exceptional mechanical properties.<sup>1-9</sup> This has motivated extensive research for the potential applications of CNT's as the reinforcements of a new generation of composites, including the theoretical evaluations of the elastic properties of CNT's, the improvement of the wetting and adhesion between CNT's and matrix, the uniform dispersion of CNT's within the matrix and so on. It is noticed that many theoretical models were proposed for the elastic moduli of single-walled carbon nanotubes (SWNT's), such as the molecular dynamics and molecular mechanics based on empirical potentials,<sup>10-21</sup> the tight-binding-based approaches,<sup>22-26</sup> the first principles of quantum mechanics,<sup>27-29</sup> the continuum mechanics models,<sup>30,31</sup> and the structure mechanics model.<sup>32-34</sup> In contrast to the achievements for SWNT's, there were only a few numerical calculations for the selected elastic moduli of multiwalled carbon nanotubes (MWNT's).<sup>14,35,36</sup> Therefore, a complete set of five independent elastic moduli of MWNT's are the focus in the study.

The axial Young's modulus of MWNT's was experimentally measured. The reported values are 0.40–4.15 TPa with an average of 1.8 TPa (Ref. 1), 0.69–1.87 TPa with an average of 1.28 TPa (Ref. 2), 1 TPa (Ref. 3), 1.7–2.4 TPa (Ref. 4), 0.22–0.68 TPa (Ref. 6), and 270–950 GPa (Ref. 9). The various uncertainties involved in the experimental tests may be responsible for the variations of the measured axial Young's modulus of MWNT's. For example, the contributions of inner tubes were not well distinguished in these experimental measurements. In principle, the effective axial Young's modulus of MWNT's must be larger than that of SWNT's. Furthermore, the technical difficulty makes the ex-

perimental determination of other elastic moduli, such as Poisson's ratio and bulk and shear moduli, a rather challenging task. Also, it is difficult to experimentally investigate the effect of structural parameters of MWNT's, such as chirality on the elastic properties. For SWNT's, the closed-form expressions for the five independent elastic moduli of SWNT's were obtained.<sup>21</sup> However, only a few numerical simulations were reported for some selected elastic moduli of MWNT's due to the increased complexity.<sup>14,35,36</sup> For example, the axial Young's and torsional shear moduli and major Poisson's ratio were numerically obtained as about 0.97 TPa, 0.45 TPa, and 0.28 using the empirical force-constant model, and it was concluded that the wall numbers and interwall van der Waals forces have a little or no significant effects on the elastic moduli.<sup>14</sup> The axial Young's and torsional shear moduli were simulated using the molecular structural mechanics method and numerically obtained as 1.05 and 0.4 TPa.<sup>35</sup> Also, it was demonstrated that the inner tubes only have a little effect on the moduli if the loadings are not directly exerted on inner tubes. It is not clear how long MWNT's were used in these numerical simulations. In fact, a complete shear stress transfer among tubes through van der Waals forces requires a certain length, while the capillary force or retract force is dominant for short tubes.<sup>37</sup> So, if the MWNT length is not enough long, the loadings exerted on the outermost tube cannot be effectively transferred onto the inner tubes.

Motivated by the achievement of the closed-form expressions of the five independent effective elastic moduli of SWNT's,<sup>21</sup> the authors attempt to find the corresponding results for MWNT's in the study. Compared with the SWNT's, the situation of MWNT's further involves the analysis for the van der Waals forces that transfer the stresses among tubes, the different distributions of the tensile loading at the ends of all tubes, and the dependence of the longitudinal Young's and shear moduli on the MWNT length. These troublesome prob-

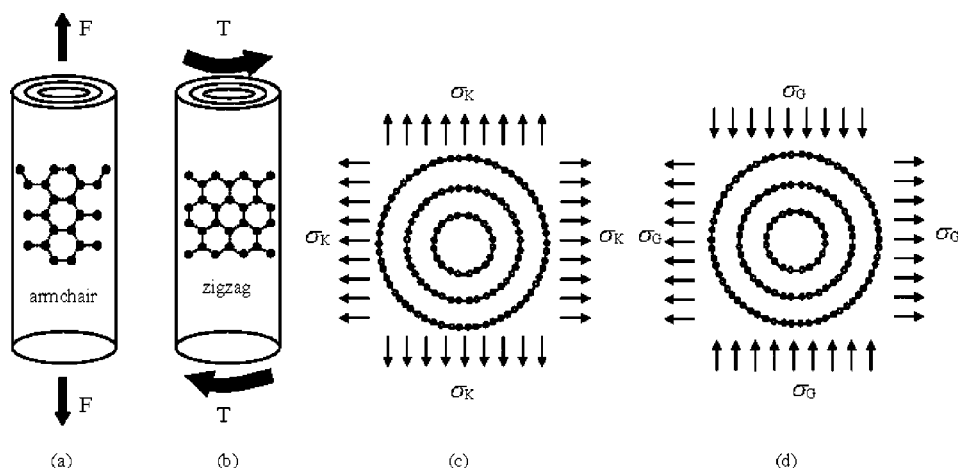


FIG. 1. Four types of loading conditions: (a) axial tension, (b) torsional moment, (c) in-plane biaxial tension, and (d) tension-compression stress.

lems have not been well analyzed in the literature. Some assumptions without a significant loss of accuracy are proposed in order to get the analytical expressions of the five independent elastic moduli of MWNT's. Based on them, the effects of the wall number, diameter, chirality, length of MWNT's, and the tension loading distributions are clearly displayed and discussed.

## II. ELASTIC MODULI OF A MWNT

When a MWNT with  $N$  walls is used as an entity, such as the reinforcement of composites, the effective elastic properties of the MWNT need to be obtained first. Due to its structural features, its effective elastic properties are transversely isotropic. Therefore, five independent elastic moduli are needed to describe its transversely isotropic behavior completely.

In this study, five independent effective elastic moduli such as the longitudinal Young's modulus, major Poisson's ratio, longitudinal shear modulus and plane-strain bulk and in-plane shear moduli, respectively, denoted as  $\bar{E}_{11}$ ,  $\bar{\nu}_{12}$ ,  $\bar{G}_{12}$ ,  $\bar{K}_{23}$ , and  $\bar{G}_{23}$  are taken by assuming  $l$  as the longitudinal or axial direction along the tube. They are defined by visualizing the MWNT as a solid cylinder with the same radius. Because an individual consideration for the interaction between the MWNT and matrix of composites is necessary, the radius is determined from the tube center to the atoms of the outermost tube.

The four loading conditions are chosen to determine the five effective elastic moduli. They are the axial loading  $F$  for  $\bar{E}_{11}$  and  $\bar{\nu}_{12}$ , torsional moment  $T$  for  $\bar{G}_{12}$ , in-plane biaxial tension with magnitude  $\sigma_K$  for  $\bar{K}_{23}$ , and tension-compression stress (pure shear stress) with magnitude  $\sigma_G$  for  $\bar{G}_{23}$ , as shown in Figs. 1(a)–1(d).

It is noticed that for the two cases of the axial loading, i.e., the axial tensile and compressive loading, the contributions of the inner tubes to the elongation of MWNT's are different, resulting in different Young's moduli. Correspondingly, the terms tensile and compressive Young's moduli are named.

When the axial loading is tensile, the loading transferred onto inner tubes comes from three contributions: the interaction between caps, capillary force and interlayer shear stress.

The former two only work around the ends of MWNT's, while the latter one distributes along the tubes and depends on the tube length. It can be imagined that the interaction force between caps is very small due to the small contact area at caps, and it will disappear due to a small elongation difference between the outer and inner tubes at the caps. Also, the capillary force is small, which can reach a constant value, say about 1 nN for the pair of (5,5) (10,10) tubes.<sup>37</sup> So, in the initial stage of loading-displacement curve, say the tensile loading varying from 0 to 2 nN, the two forces will significantly increase the slope of the loading-displacement curve. But after the initial stage, two forces will have no effect on the loading-displacement curve because they do not increase further. The experiment for the simple tension of MWNT's showed that before the outermost tube breaks, the tensile loading can reach several hundreds of nN and the loading-displacement curve approximately remains linear in trends.<sup>9</sup> So, when the axial Young's modulus is used to characterize the average slope of the loading-displacement curve in a wide range, the small initial stage can be neglected for the simplicity of theoretical analysis, i.e., MWNT's are modeled as concentric cylindrical shells without caps and the interlayer shear stress is only considered for the loading transfer from outer to inner tubes.

When the axial loading is compressive, the caps of outer and inner tubes always join together, resulting in the same axial displacements for all tubes. So, when the caps are neglected, a uniform end displacement condition for all tubes should be assumed, which approximately corresponds to a uniform distribution of axial loading on all the ends of tubes.

Each tube within a MWNT is treated as a SWNT, which is also transversely isotropic. For SWNT's, three different definitions for Young's modulus and torsional (or longitudinal) shear modulus have been named for various purposes, which are denoted as  $E_{11}^s$  and  $G_{12}^s$ ,  $E_{11}$  and  $G_{12}$ , and  $\bar{E}_{11}$  and  $\bar{G}_{12}$ . The surface Young's and longitudinal shear moduli,  $E_{11}^s$  and  $G_{12}^s$  do not involve the tube thickness.<sup>19,21</sup> The conventional moduli  $E_{11}$  and  $G_{12}$  are based on a tube thickness  $t$ . And the effective moduli  $\bar{E}_{11}$  and  $\bar{G}_{12}$  are based on the cross-sectional area of tube.<sup>21</sup> The elastic moduli based on the three definitions are related to each other through  $E_{11} = E_{11}^s/t$  and  $G_{12} = G_{12}^s/t$ , and  $\bar{E}_{11} = E_{11}^s/(R/2)$  and  $\bar{G}_{12} = G_{12}^s/(R/2)$ , where  $R$  is the tube radius.

The purpose to define the area-based moduli is for the convenience of considering the stiffening effect of CNT's on composites. The other three moduli, i.e., the major Poisson's ratio, plane-strain bulk modulus, and in-plane shear modulus, denoted as  $\nu_{12}$ ,  $K_{23}$ , and  $G_{23}$  for SWNT's do not involve the tube thickness because they do not involve how to define the average value of external loading over the cross-sectional area of the tube.

The closed-form expressions for the five elastic moduli of the  $m$ th SWNT, i.e.,  $E_{11,m}^s$ ,  $\nu_{12,m}$ ,  $G_{12,m}^s$ ,  $K_{23,m}$ , and  $G_{23,m}$  are available,<sup>21</sup> where the subscript  $m$  is added to denote the properties associated with the  $m$ th tube counted from the outermost one.

There are three basic interwall deformation modes, i.e., two shear deformations in axial and circumferential directions and one normal deformation in radial direction. A linear elastic interwall stress-strain relation corresponding to each deformation mode can be used due to small strain condition.

For the four loading conditions, i.e., axial loading, torsional moment, in-plane biaxial tension, and tension-compression stress, the four corresponding interwall deformation modes of a MWNT are the combination of the axial shear and radial normal strains, the circumferential shear strain, the radial normal strain, and the combination of the circumferential shear and radial normal strains, respectively. The global deformations of the MWNT under each loading can be obtained using elasticity theory. Then, the corresponding elastic moduli can be extracted based on their traditional definitions by visualizing the MWNT as a solid cylinder or a hollow one.

### A. Longitudinal Young's modulus and major Poisson's ratio

The axial tension loading shown in Fig. 1(a) is used to analyze the longitudinal Young's modulus and major Poisson's ratio of a  $N$ -walled MWNT with length of  $2L$ . Figure 2 is a schematic diagram to show the analysis of deformations and stresses in the axial direction for a small segment  $P_m Q_m P_{m+1} Q_{m+1}$  from  $x$  to  $x+dx$  of the  $m$ th and  $(m+1)$ th tubes, where  $m$  is counted from the outermost tube. The stresses  $\tau_{m,i}(x)$  and  $\tau_{m,o}(x)$ , and  $\sigma_{m,i}(x)$  and  $\sigma_{m,o}(x)$  denote the shear and normal stresses acting on the inner and outer sides of the  $m$ th tube due to the variation of the interwall van der Waals forces. The symbols  $h_m$ ,  $\gamma_m(x)$ , and  $\varepsilon_m(x)$  denote the  $m$ th interwall distance, the  $m$ th interwall shear strain, and normal strain, respectively.  $f_m(x)$  and  $f_{\theta,m}(x)$  are the axial and circumferential forces per unit length within the  $m$ th tube at the location  $x \in [0, L]$ , where  $L$  is the half length of the MWNT.

Let  $u_m(x)$  and  $v_m(x)$ , and  $\varepsilon_{11,m}(x)$  and  $\varepsilon_{22,m}(x)$  be the axial and radial displacements and strains of the  $m$ th tube, and  $R_m$  denote the radius of the  $m$ th tube. The controlling equations of the stresses and deformations of the system are given as follows.

#### 1. The force balance equations

As shown in Fig. 2(a), the force balances of the outer and inner tubes, i.e.,  $P_m Q_m$  and  $P_{m+1} Q_{m+1}$ , and the two tubes, i.e.,  $P_m Q_m Q_{m+1} P_{m+1}$  as an entity in the axial direction, can lead to

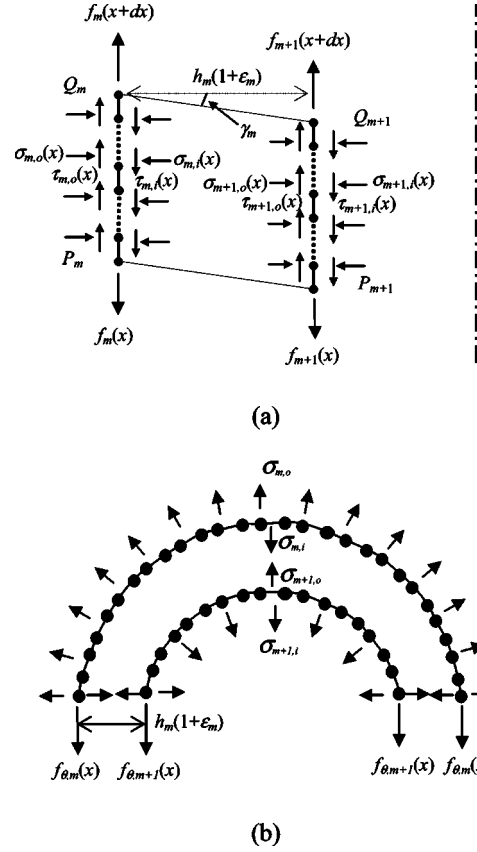


FIG. 2. Schematic diagrams for the stresses and deformations of a small segment of two tubes with MWNT's under tension loading condition, (a) for the axial analysis and (b) for the radial analysis.

$$\frac{df_m(x)}{dx} = \tau_{m,o}(x) - \tau_{m,i}(x) \quad (1)$$

and

$$\sigma_{m,i}(x)R_m = \sigma_{m+1,o}(x)R_{m+1}. \quad (2)$$

As shown in Fig. 2(b), the force balances of the half ring of outer and inner tubes, and the two half rings of tubes as an entity in the vertical direction of the figure, can lead to

$$f_{\theta,m}(x) = R[\sigma_{m,o}(x) - \sigma_{m,i}(x)], \quad (3)$$

$$\tau_{m,i}(x)R_m = \tau_{m+1,o}(x)R_{m+1}. \quad (4)$$

The interwall stress variation from one side to the other of the interwall region expressed by Eqs. (2) and (4) shows that the interwall stresses are inversely proportional to the tube radius. It is noted that a similar equation to Eq. (2) was directly assumed without rigorous proof.<sup>38</sup>

### 2. The stress-strain relations

Taking the  $m$ th tube as a SWNT and using its surface longitudinal Young's modulus, plane-strain bulk modulus, and major Poisson's ratio, i.e.,  $E_{11,m}^s$ ,  $K_{23,m}$  and  $\nu_{12,m}$ ,<sup>21</sup> the stress-strain relations for the tube shell can be derived as follows:

$$\varepsilon_{11,m}(x) = \frac{1}{E_{11,m}^s} [f_m(x) - \nu_{12,m} f_{\theta,m}(x)], \quad (5)$$

$$\varepsilon_{22,m}(x) = \frac{1}{E_{11,m}^s} [\lambda f_{\theta,m}(x) - \nu_{12,m} f_m(x)], \quad (6)$$

where  $\lambda = \nu_{12,m}^2 + E_{11,m}^s / (2R_m K_{23,m})$ .

The interwall normal and shear stresses caused by the variation of the interwall van der Waals forces can be generally assumed to be a function of the interwall normal and shear strains as follows:

$$\sigma_m(x) = \Phi_m(\varepsilon_m(x)), \quad (7)$$

$$\tau_m(x) = \Psi_m(\gamma_m(x)), \quad (8)$$

where  $\sigma_m(x)$  and  $\tau_m(x)$  denote the average normal and shear stresses within the interwall region with

$$\sigma_m(x) = \frac{2R_m \sigma_{m,i}(x)}{R_m + R_{m+1}}$$

and

$$\tau_m(x) = \frac{2R_m \tau_{m,i}(x)}{R_m + R_{m+1}},$$

$\Phi_m(\varepsilon_m)$  and  $\Psi_m(\gamma_m)$  are nonlinear functions of the interwall strains and they should be dependent on the curvatures of the tubes and the commensuration between tubes. In principle, they may be derived using the Lennard-Jones model.<sup>39</sup>

### 3. The geometry equations

The interwall normal and shear strains  $\varepsilon_m(x)$  and  $\gamma_m(x)$  and the tube strains  $\varepsilon_{11,m}(x)$  and  $\varepsilon_{22,m}(x)$  can be related to the displacements  $u_m(x)$  and  $v_m(x)$  as follows:

$$\varepsilon_m(x) = [v_m(x) - v_{m+1}(x)]/h_m, \quad (9)$$

$$\gamma_m(x) = [u_m(x) - u_{m+1}(x)]/h_m, \quad (10)$$

$$\varepsilon_{11,m}(x) = du_m(x)/dx, \quad (11)$$

$$\varepsilon_{22,m}(x) = v_m(x)/R_m. \quad (12)$$

### 4. The boundary conditions

The free stress condition on the outside of the outermost tube and the inside of the innermost tube gives

$$\sigma_{1,o}(x) = 0, \quad \tau_{1,o}(x) = 0,$$

$$\sigma_{N,i}(x) = 0, \quad \tau_{N,i}(x) = 0. \quad (13)$$

The end loading condition for the distribution on the outmost tube is as follows:

$$f_1(L) = F/(2\pi R_1), \quad f_m(L) = 0 \quad (14)$$

The symmetric condition at the middle of the MWNT gives

$$u_m(0) = 0, \quad df_m(x)/dx|_{x=0} = 0. \quad (15)$$

### 5. Solving the controlling equations of the system

As the small-strain condition is of concern for the elastic properties, the nonlinear interwall stress-strain relations (7) and (8) can be linearized by neglecting the higher orders of terms in Taylor's expansion of the functions  $\Phi_m(\varepsilon_m)$  and  $\Psi_m(\gamma_m)$  as follows:

$$\sigma_m(x) = E_m \varepsilon_m(x), \quad (16)$$

$$\tau_m(x) = G_m \gamma_m(x), \quad (17)$$

where the constant  $E_m$  and  $G_m$  are referred to as the interwall Young's and shear moduli in the radial and axial directions, which are dependent on the curvature of tubes and the commensuration between the tubes. Especially, the commensuration between tubes is more important for the magnitude of the two constants.<sup>40,41</sup>

The axial and radial stresses and deformations are coupled due to the coupled stress-strain relations (5) and (6). However, the circumferential stress  $f_{\theta,m}(x)$  is much smaller than the axial stress  $f_m(x)$ , as it is caused by the difference of the two weak interwall normal stresses. For simplicity,  $f_{\theta,m}(x)$  in Eq. (5) is neglected so that the controlling equations (1)–(15) of the system become uncoupled for the axial and radial analyses.

For the axial analysis, Eqs. (1), (4), (5), (10), (11), and (17) consist of the controlling equations for the unknown variables  $f_m(x)$ ,  $\tau_{m,i}(x)$ ,  $\tau_{m,o}(x)$ ,  $\varepsilon_{11,m}(x)$ ,  $\gamma_m(x)$ , and  $u_m(x)$ . For the case of a double-walled carbon nanotube (DWNT), a second-order ordinary differential equation for the unknown variable  $f_1(x)$  can be derived from these equations through the substituting and eliminating procedures. Then, based on the boundary conditions (13)–(15), the explicit solution of  $f_1(x)$  can be obtained. And then, other variables can be obtained using the solution of  $f_1(x)$ . For example,  $\tau_1(x)$  can be obtained from Eq. (1), while  $u_1(x)$  is obtained from Eqs. (11) and (5) with the boundary condition (15).

For the radial analysis, Eqs. (2), (3), (6), (9), (12), and (16) with the boundary conditions (13) consist of a set of linear equations for the unknown variables  $f_{\theta,m}(x)$ ,  $\sigma_{m,i}(x)$ ,  $\sigma_{m,o}(x)$ ,  $\varepsilon_{22,m}(x)$ ,  $\varepsilon_m(x)$ , and  $v_m(x)$ , which can be easily solved. It is noted that  $f_m(x)$  in Eq. (6) has been obtained from the axial analysis.

For the case of DWNT, the analytical expression of the interwall shear stress  $\tau_1(x)$ , is given as

$$\tau_1(x) = \frac{2f_1 \sqrt{A} R_1 / (R_1 + R_2)}{1 + (E_{11,1}^s R_1) / (E_{11,2}^s R_2)} \left( \frac{e^{x\sqrt{A}}}{e^{2L\sqrt{A}} + 1} - \frac{e^{-x\sqrt{A}}}{e^{-2L\sqrt{A}} + 1} \right), \quad (18)$$

with

$$A = \frac{1}{2} \left( 1 + \frac{R_2}{R_1} \right) \left( \frac{1}{E_{11,1}^s} + \frac{R_1}{R_2} \frac{2}{E_{11,2}^s} \right) \frac{G_1}{h_1}. \quad (19)$$

Using the solution of the end displacement  $u_1(L)$  of the outer tube and defining the effective longitudinal Young's modulus of the DWNT as  $\bar{E}_{11} = (F/\pi R_1^2)/(u_1(L)/L)$  by visualizing it as a solid cylinder,  $\bar{E}_{11}$  is obtained as

$$\bar{E}_{11} = \frac{2E_{11,1}^S}{R_1} \left[ 1 + \frac{E_{11,2}^S R_2 (1-B)}{E_{11,1}^S R_1 + E_{11,2}^S R_2 B} \right], \quad (20)$$

with

$$B = \frac{1}{L\sqrt{A}} \frac{e^{2L\sqrt{A}} - 1}{e^{2L\sqrt{A}} + 1}. \quad (21)$$

Using the solution of the radial displacement  $v_1(x)$  of the outer tube and defining the effective major Poisson's ratio  $\bar{\nu}_{12}$  as the average ratio of the radial and axial strains,  $\bar{\nu}_{12}$  is obtained as

$$\bar{\nu}_{12} = \nu_{12,1}(1 - \eta), \quad (22)$$

where

$$\eta = \frac{[1 - (R_2/R_1)(\nu_{12,2}/\nu_{12,1})\xi]E_1 R_1 / (h_1 K_{23,1})}{1 + R_1/R_2 + (R_1/K_{23,1} + R_2/K_{23,2})E_1/h_1}. \quad (23)$$

and

$$\xi = \frac{1}{L} \int_0^L \frac{1 - \frac{e^{\sqrt{A}x}}{1 + e^{2L\sqrt{A}}} - \frac{e^{-\sqrt{A}x}}{1 + e^{-2L\sqrt{A}}}}{1 + \frac{E_{11,2}^S R_2}{E_{11,1}^S R_1} \left( \frac{e^{\sqrt{A}x}}{1 + e^{2L\sqrt{A}}} + \frac{e^{-\sqrt{A}x}}{1 + e^{-2L\sqrt{A}}} \right)} dx. \quad (24)$$

For the two special cases of  $L \rightarrow 0$  and  $L \rightarrow \infty$ , the parameter  $B$  expressed in Eq. (21) becomes 1 and 0, while the parameter  $\xi$  in Eq. (24) becomes 0 and 1.

For the cases of MWNT's, numerical methods are needed to solve the set of controlling equations accurately. However, based on the solution of DWNT's, a replacement method can be approximately used without significant loss of accuracy. The replacement procedure is that the innermost two tubes are analyzed based on the solution for DWNT's first, then using its elastic moduli to replace those of the inner tube in the solution for DWNT's and taking the elastic moduli of the next tube as those of the outer tube, the elastic moduli of the innermost three tubes is derived. The procedure can be done until the outermost tube.

For the case of compressive loading, the boundary conditions at the ends of tubes, i.e., Eq. (14), should be changed to a uniform end displacement condition. Due to the consistent axial displacements for all tubes, the interwall shear deformation and shear stress vanish, resulting in the constant axial inner force from Eq. (1). Therefore, the controlling equations reduce to a set of linear equations, which can be easily solved. It is obtained that the effective compressive longitudinal Young's modulus and major Poisson's ratio are independent of the MWNT length for this case, that is,

$$\bar{E}_{11} = \frac{2}{R_1^2} \sum_{i=1}^N R_i E_{11,i}^S, \quad (25)$$

$$\bar{\nu}_{12} = \frac{(\nu_{12,1} R_1 - \nu_{12,2} R_2) E_1 / (h_1 K_{23,1})}{1 + R_1/R_2 + (R_1/K_{23,1} + R_2/K_{23,2}) E_1 / h_1}. \quad (26)$$

The expressions are consistent with those of the tensile loading, i.e., Eqs. (20) and (22) in the limiting case of  $L \rightarrow \infty$ . It is

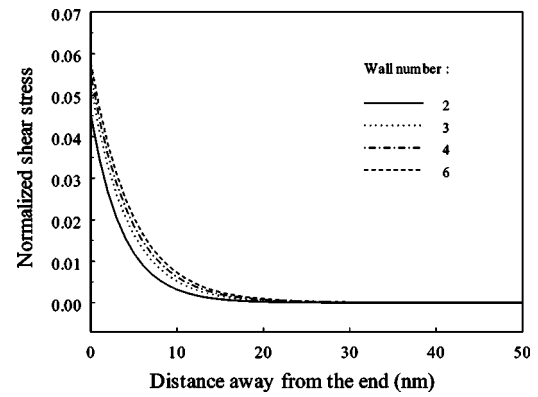


FIG. 3. Variations of the outermost interwall shear stress for various wall numbers.

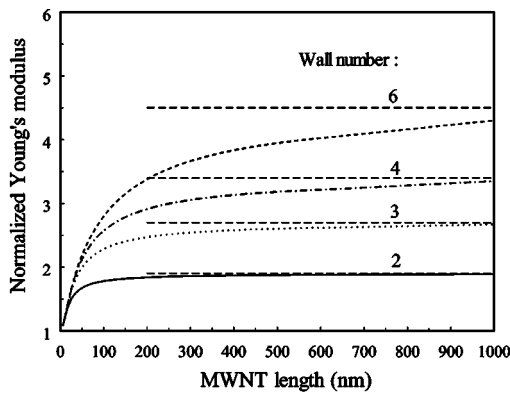
noticed that Eq. (26) accounts for the effect of interwall distance changes, which is derived using the same controlling equations for the case of tensile loading, i.e., Eqs. (2), (3), (6), (9), (12), and (16).

As an example of application, these expressions for MWNT's composed of armchair tubes are plotted with all the interwall distances  $h_m$  being assumed as 0.34 nm. The tubes within such MWNT's are axially commensurate.<sup>42,43</sup> But their commensuration in circumferential direction may become loose as the tube curvature increase. It can be envisioned that when the curvature of tubes approaches zero or the tube diameter is sufficiently large, the interaction between two adjacent armchair tubes will reduce to that in graphite. For simplicity, the curvature effect is neglected in the preliminary study, and  $E_m$  and  $G_m$  are assumed to be the same as those of graphite, i.e., the elastic moduli  $c_{33}$  and  $c_{44}$  of graphite in normal and interlayer directions, which have been extensively measured. The experimental values of  $c_{33}$  from different researchers do not vary widely, which is taken as  $c_{33}=0.0365$  TPa.<sup>44</sup> But the values of  $c_{44}$  vary in a large range for different experimental tests, and it can increase about 20 times after neutron irradiation. Here a relatively large value of  $c_{44}=0.0039$  TPa from Ref. 44 is used for the plotting of the analytical expressions. It is noted that the values may overestimate the two constants even for the commensurate MWNT's.<sup>40,41</sup>

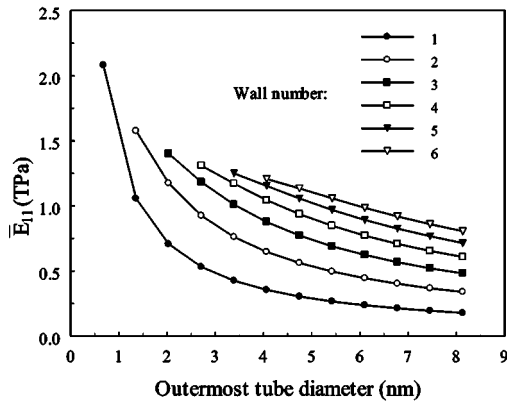
The variations of the outermost interwall shear stress for various wall numbers are plotted in Fig. 3. It is seen that a complete stress transfer needs the MWNT length to be greater than about 30 nm.

Figure 4(a) shows the dependence of the tensile and compressive longitudinal Young's moduli on the MWNT length for various wall numbers, in which the horizontal lines correspond to the compressive Young's modulus. It is seen that when the length of MWNT is greater than 1000 nm, the tensile Young's modulus is close to its stable value or the compressive Young's modulus. Figure 4(b) shows the dependence of the stable value of tensile Young's modulus on the wall number and diameter of MWNT's.

The variations of the major Poisson's ratio with MWNT length for various wall numbers are plotted in Fig. 5(a). Figure 5(b) shows its dependence on the wall number and diameter of MWNT's with very long length. It is noted that the



(a)



(b)

FIG. 4. (a) The dependence of the effective longitudinal tensile Young's modulus on the MWNT length for various wall numbers, which is normalized by that of the outermost tube; (b) the dependence of the stable value of the tensile Young's modulus on the wall number and diameter of MWNT's.

outermost tube is fixed as the (50,50) armchair tube for Figs. 3, 4(a), and 5(a) when checking the MWNT length effect.

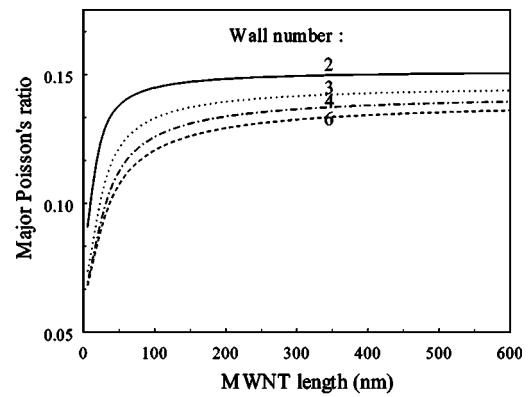
**B. Longitudinal shear modulus**

The longitudinal shear modulus of a solid cylinder with transversely isotropic elastic properties is only relevant to the torsional angle of the cylinder subjected to a torque. So the longitudinal shear modulus of a MWNT can be extracted by analyzing the torsional angle of the MWNT subjected to a torque  $T$ , as shown in Fig. 1(b).

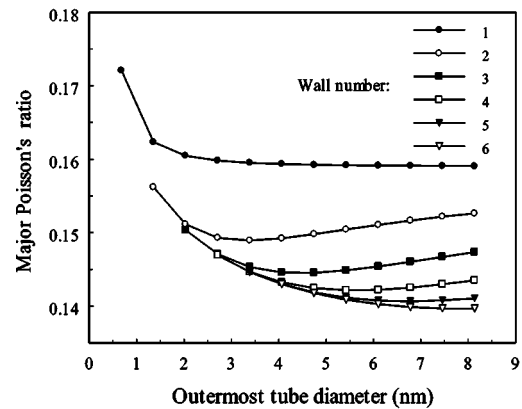
It is assumed that the torque  $T$  is applied on the outermost wall of the MWNT. The loading is transferred to the inner tubes through the shear stress in the circumferential direction caused by the variation of the interwall van der Waals forces corresponding to the relative torsion among tubes.

Figure 6 is a schematic diagram to show the stresses and deformations of two adjacent tubes. Based on the torque balances of the outer and inner tubes, and the two tubes as an entity, the relation between the shear stresses at the two sides of the interwall region can be obtained as

$$\tau_{m,i}(x)R_m^2 = \tau_{m+1,o}(x)R_{m+1}^2. \quad (27)$$



(a)



(b)

FIG. 5. (a) The dependence of the major Poisson's ratio on the MWNT length for various wall numbers; (b) the dependence of the major Poisson's ratio on the wall number and diameter of MWNT's.

For the shear and normal deformation modes in the axial and radial directions, Eqs. (2) and (4) show an inversely linear variation of interwall shear and normal stresses with the tube radius in the two sides of interwall region. However, for the shear deformation mode in the circumferential direction, Eq. (27) shows an inverse variation of interwall shear stress to the squared tube radius. In contrast, the squared variation is not so intuitive.

The other controlling equations for a MWNT under the torque are similar to those in the axial analysis if  $E_{11,m}^s$ ,  $G_m$ ,

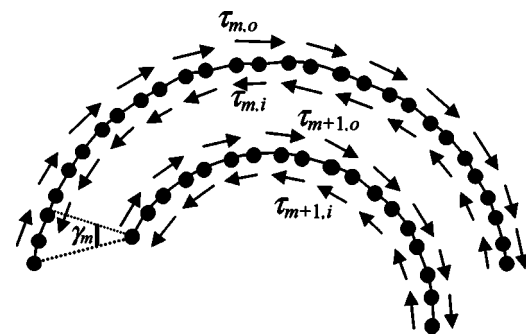


FIG. 6. A schematic diagram to show the stresses and deformations of two adjacent tubes under torsional moment loading.

and  $f_1(L)=F/(2\pi R_1)$  are replaced by  $R_m G_{12,m}^s$ ,  $R_m G_m$ , and  $f_1(L)=T/(2\pi R_1^2)$  and  $u_m(x)$  and  $f_m(x)$  are understood as the torsional angle  $\theta_m(x)$  and the shear force  $f_{\theta,m}(x)$  per length within the  $m$ th tube.

For the case of DWNT, using the solution of the torsional angle  $\theta_1(L)$  at the end of the outermost tube and defining the effective longitudinal shear modulus as  $\bar{G}_{12} = TL/[\pi R_1^4 \theta_1(L)]$ ,  $\bar{G}_{12}$  is similarly obtained as

$$\bar{G}_{12} = \bar{G}_{12,1} \left[ 1 + \frac{G_{12,2}^s R_2^3 (1-B)}{G_{12,1}^s R_1^3 + G_{12,2}^s R_2^3 B} \right], \quad (28)$$

with

$$B = \frac{1}{L\sqrt{A}} \frac{e^{2L\sqrt{A}} - 1}{e^{2L\sqrt{A}} + 1} \quad (29)$$

and

$$A = \frac{1}{4} \left( 1 + \frac{R_2}{R_1} \right)^2 \left( \frac{1}{G_{12,1}^s} + \frac{R_1^3}{R_2^3} \frac{1}{G_{12,2}^s} \right) \frac{G_1}{h_1}, \quad (30)$$

where  $G_{11,1}^s$  and  $G_{11,2}^s$  are the surface longitudinal shear moduli of the outer and inner tubes, and  $G_1$  is the interwall shear modulus in circumferential direction, which is also assumed to be the same as  $c_{44}$  of graphite when plotting the expression (28).

For a MWNT, the replacement procedure is similarly used to derive its  $\bar{G}_{12}$  based on the solution of DWNT's. The dependence of the longitudinal shear modulus on the MWNT length for various wall numbers is shown in Fig. 7(a) where the outermost tube is also fixed as (50,50) armchair tube. It is seen that when the length of MWNT is greater than 1000 nm, the longitudinal shear modulus is close to its stable value. Due to  $B=0$  when  $L \rightarrow \infty$ , the stable value of the longitudinal shear modulus for a MWNT can be obtained as

$$\bar{G}_{12} = \frac{2}{R_1^4} \sum_{i=1}^N R_i^3 G_{12,i}^s. \quad (31)$$

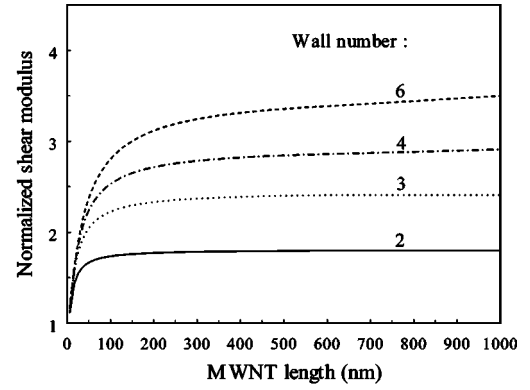
Figure 7(b) shows the dependence of the longitudinal shear modulus on the wall number and diameter of MWNT's.

### C. Plane-strain bulk modulus

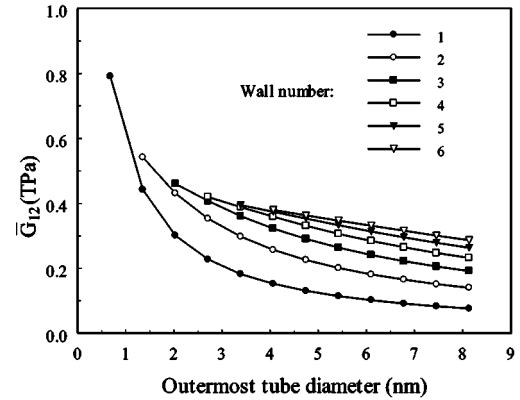
A DWNT subjected to the two-dimensional plane-strain condition of biaxial tension stresses with magnitude  $\sigma_K$  is analyzed to get its plane-strain bulk modulus, as shown in Fig. 1(c). Based on the axisymmetric condition, the radial displacements  $v_1$  and  $v_2$  of the outer and inner tubes can be used to characterize the deformation of the DWNT. The interwall normal strain  $\varepsilon_1$  is related to the displacements  $v_1$  and  $v_2$  as follows:

$$\varepsilon_1 = (v_1 - v_2)/h_1. \quad (32)$$

The outer tube is subjected to the biaxial stresses  $\sigma_K$  in its outside and the biaxial interwall stress  $\sigma_1$  in its inside, while the inner tube is subjected to the biaxial interwall stress  $\sigma_2$  in its outside. According to the deformation of each SWNT under the biaxial stresses, the following two equations can be obtained:



(a)



(b)

FIG. 7. (a) The dependence of the longitudinal shear modulus on the MWNT length for various wall numbers, (b) the dependence of the longitudinal shear modulus on the wall number and diameter of MWNT's.

$$2\nu_1/R_1 = 2\varepsilon_{22,1} = (\sigma_K - \sigma_1)/K_{23,1} \quad (33)$$

and

$$2\nu_2/R_2 = 2\varepsilon_{22,2} = \sigma_2/K_{23,2}, \quad (34)$$

where  $\varepsilon_{22,1}$  and  $\varepsilon_{22,2}$  are the radial strains of the outer and inner tubes.

The radial strain  $\varepsilon_{22,1}$  of the outer tube can be obtained using Eqs. (32)–(34) together with Eqs. (2) and (16). Then, based on the definition of the effective plane-strain bulk modulus, i.e.,  $\bar{K}_{23} = \sigma_K/(2\varepsilon_{22,1})$ ,  $\bar{K}_{23}$  of the DWNT can be obtained as

$$\bar{K}_{23} = \bar{K}_{23,1}(1 + \eta_K), \quad (35)$$

with

$$\eta_K = \frac{E_1/K_{23,1}}{E_1/K_{23,2} + 4h_1/(R_1 + R_2)}. \quad (36)$$

For a MWNT, the replacement procedure can be exactly used to derive its  $\bar{K}_{23}$  based on the solution of DWNT's. The variation of the plane-strain bulk modulus  $\bar{K}_{23}$  with the outermost diameter of MWNT's for various wall numbers is plotted in Fig. 8.

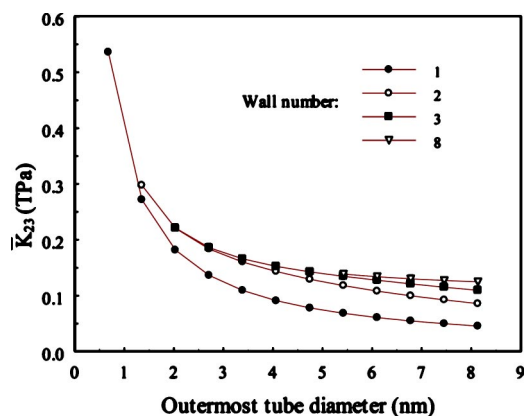


FIG. 8. The dependence of the plane-strain bulk modulus on the wall number and diameter of MWNT's.

#### D. In-plane shear modulus

For a DWNT subjected to tension-compression loading, as shown in Fig. 1(d), it is assumed that the inner tube is also subjected to a tension-compression loading, which is transferred through the van der Waals forces due to the interwall distance changes. So, based on the analysis of each tube, its outer and inner circular cross-sectional perimeters are assumed to bend into elliptic ones, as shown in Fig. 9. The two unknown strains  $\varepsilon_1$  and  $\varepsilon_2$  characterize the deformations from the circles with radii  $R_1$  and  $R_2$  to the ellipses with longer and shorter half-axis  $R_1(1+\varepsilon_1)$  and  $R(1-\varepsilon_1)$ , and  $R_2(1+\varepsilon_2)$  and  $R_2(1-\varepsilon_2)$ . Due to the symmetric condition, the interwall shear strains at the longer and shorter axis are zero and the normal strains are expressed as  $(\varepsilon_1 R_1 - \varepsilon_2 R_2)/h_1$  and  $(-\varepsilon_1 R_1 + \varepsilon_2 R_2)/h_1$ . Let  $\sigma_1$  and  $\sigma_2$  denote the magnitudes of the interwall tension-compression stresses acting on the inside of the outer tube and the outside of the inner tube at the locations of the longer and shorter axis. By analyzing the interwall normal stresses and strains at these symmetric locations of the ellipses and referring to Eq. (16), the relation between the interwall stresses and strains can be obtained as follows:

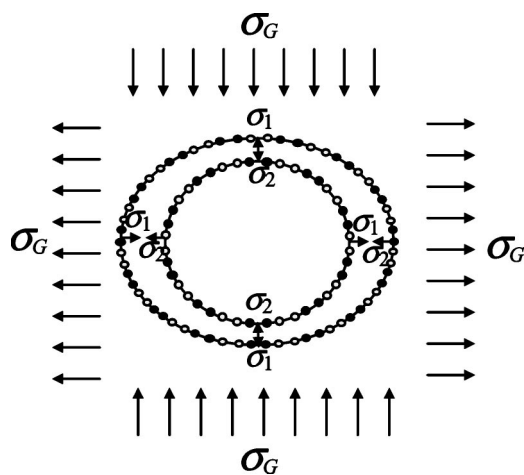


FIG. 9. A schematic diagram to show the shape changes from circles to ellipse of the outer and inner tubes.

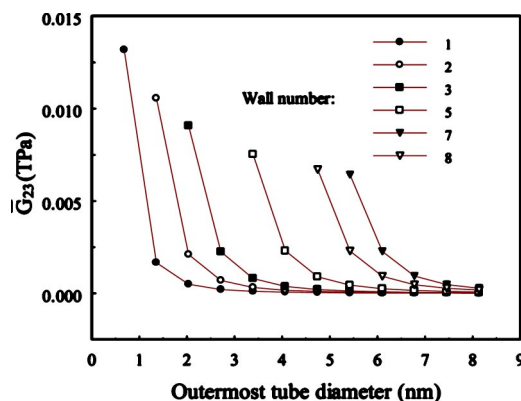


FIG. 10. The dependence of the in-plane shear modulus on the wall number and diameter of MWNT's.

$$(\sigma_1 + \sigma_2)/2 = E_1(\varepsilon_1 R_1 - \varepsilon_2 R_2)/h_1. \quad (37)$$

According to the in-plane relation between stress and strain of each SWNT under a tension-compression loading, the following two equations can be obtained:

$$2\varepsilon_1 = (\sigma_G - \sigma_1)/G_{23,1} \quad 2\varepsilon_2 = \sigma_2/G_{23,2}, \quad (38)$$

where  $G_{23,1}$  and  $G_{23,2}$  denote the in-plane shear moduli of the outer and inner tubes. Equations (37), (38), (2), and (16) together with the definition of the in-plane shear modulus, i.e.,  $\bar{G}_{23} = \sigma_G / (2\varepsilon_1)$  can lead to

$$\bar{G}_{23} = G_{23,1} + \frac{E_1 G_{23,2} (R_1 + R_2)}{E_1 (R_1 + R_2) + 4G_{23,2} h_1}. \quad (39)$$

For a MWNT with more walls, the replacement procedure can be approximately used to derive its  $\bar{G}_{23}$  based on the solution of DWNT's. The variation of the in-plane shear modulus  $\bar{G}_{23}$  with the outermost diameter of MWNT's for various wall numbers is plotted in Fig. 10.

### III. DISCUSSION AND REMARKS

In this paper, the analytical expressions for five independent effective elastic moduli of MWNT's subjected to the axial tension-compression stresses, torsional moment, in-plane biaxial tension, and in-plane pure shear loadings at small-strain conditions have been obtained. These expressions involve the interwall elastic constants, i.e.,  $E_m$  and  $G_m$ , which are used to describe the linear elastic relations between the interwall stresses and strains corresponding to the three basic interwall deformation modes. The interwall stresses are the average of van der Waals forces over a representative area. The interwall elastic constants may vary with the curvature of tubes and are dependent on the commensuration between the tubes,<sup>40,41</sup> and  $G_m$  may not equal for the shear deformation modes in axial and circumferential directions. So far these interwall constants have not been given due to the complexity, even though they can be theoretically derived based on the Lennard-Jones model in principle.<sup>39</sup> For simplicity, the interwall values of single-crystal graphite are approximately adopted in the present examples for MWNT composed of armchair tubes to display

TABLE I. Comparison between the five effective moduli of  $(n, n)$  SWNT's and those of MWNT composed of  $(n, n)$  SWNT's, in which the innermost tube is a (5,5) one, and the outermost tube's diameter is  $2R$ .

$n$	$2R$ (nm)	$\bar{E}_{11}$ (Tpa)		$\bar{\nu}_{12}$		$\bar{G}_{12}$ (Tpa)		$\bar{K}_{23}$ (Tpa)		$\bar{G}_{23}$ (Gpa)	
		S	M	S	M	S	M	S	M	S	M
10	1.36	1.06	1.58	0.162	0.156	0.442	0.493	0.271	0.298	1.669	10.57
15	2.04	0.707	1.41	0.161	0.150	0.301	0.398	0.181	0.221	0.496	9.073
20	2.71	0.531	1.32	0.160	0.147	0.227	0.353	0.136	0.186	0.209	8.151
25	3.39	0.425	1.27	0.160	0.145	0.182	0.327	0.109	0.166	0.107	7.520
30	4.07	0.354	1.24	0.159	0.143	0.152	0.310	0.091	0.153	0.062	7.057
35	4.75	0.304	1.21	0.159	0.142	0.131	0.298	0.078	0.145	0.039	6.699
40	5.42	0.266	1.19	0.159	0.141	0.114	0.289	0.068	0.138	0.026	6.411
45	6.10	0.236	1.18	0.159	0.140	0.102	0.282	0.061	0.134	0.018	6.175
50	6.78	0.213	1.17	0.159	0.139	0.092	0.277	0.055	0.130	0.013	5.975

the stress transfer among tubes, the length dependence, and the effect of the wall number and diameter. In order to check the effect of the approximation, an increase of the elastic constants, i.e.,  $E_m$  and  $G_m$  on the effective moduli has been checked, in which the interwall moduli increases 20% to 2% corresponding to the interwall between (5,5) and (10,10) tubes to the interwall between (45,45) and (50,50) tubes. It is found that the effects of such an increase on the effective moduli are less than 3% for the effective plane-strain bulk modulus and major Poisson's ratio, and less than 10% for the effective in-plane shear modulus. Moreover, the interwall elastic constants do not have effect on the effective longitudinal Young's and shear moduli for the two special cases of MWNT length, i.e.,  $L \rightarrow 0$  and  $L \rightarrow \infty$ , but they do have an effect on the required length, at which the longitudinal Young's and shear moduli reach their asymptotic values.

It is seen from Fig. 3 that the interwall shear stress decays away from the end of MWNT's and approaches to zero after about 30 nm, at which the stress transfer from the outer to inner tubes has finished and the deformations of all tubes have become consistent, like the situation under the tension loading associated with a uniform end displacement. As the effective longitudinal Young's modulus, major Poisson's ratio, and effective longitudinal shear modulus, i.e.,  $\bar{E}_{11}$ ,  $\bar{\nu}_{12}$ , and  $\bar{G}_{12}$  are defined based on the average values over the whole length of MWNT, they are dependent on the MWNT length and may approach to their stable values when the length is greater than about several hundreds of nanometers, depending on the wall numbers, as shown in Figs. 4(a)–7(a). Basically, the length of 1000 nm has been enough for these moduli to be very close to their stable values. For the axial loading corresponding to a uniform end displacement for all tubes, the compressive Young's modulus is obtained, which is independent of the MWNT length, and consistent with the stable value of the tensile Young's modulus. For vary short MWNT's, the tensile Young's modulus is close to the value of the outermost tube as the loading is mainly carried by the outermost tube. The effective plane-strain bulk and in-plane shear moduli, i.e.,  $\bar{K}_{23}$  and  $\bar{G}_{23}$  are independent of the MWNT length.

Also, it is seen from Figs. 4(b)–7(b), 8, and 10 and that the inner tubes may significantly increase the four effective

elastic moduli, i.e.,  $\bar{E}_{11}$ ,  $\bar{G}_{12}$ ,  $\bar{K}_{23}$ , and  $\bar{G}_{23}$ , but they decrease the major Poisson's ratio from 0.16 to 0.14. Table I lists the comparison between the effective moduli of  $(5n, 5n)$  armchair SWNT's and MWNT's with enough long length, say 1000 nm, from which the effect of inner tubes can be easily observed. It is noted that those MWNT's are composed of the series of  $(5n, 5n)$  armchair SWNT's, and their insides are fully occupied, i.e., the innermost tube is the (5,5) one. The MWNT's are called solid MWNT's here. It is seen from Table I and Fig. 10 that the in-plane shear modulus of the solid MWNT's are around 5–10 GPa, but those of the hollow ones are much lower. The radial deformation may prominently affect the electrical properties of CNT's.<sup>45,46</sup> The radial deformation and collapse of MWNT's were also observed with tapping-mode atomic force microscopy.<sup>47</sup> One observes from Fig. 10 that if MWNT's are not solid ones, their in-plane shear moduli are very low. This may be responsible for the collapse of MWNT's under in-plane loadings. The analytical expressions of the effective plane-strain bulk and in-plane shear moduli will be helpful for the analysis of the radial deformation and collapse of MWNT's with various inner and outer diameters.

One issue that needs to be emphasized is that the five effective elastic moduli are derived at small strain condition. This requires that when using them to describe the stress-strain relations of MWNT's, the magnitude of the loadings should not exceed certain critical values. However, for the tension and torsional moment loadings, the critical values that initiate the sliding deformation among tubes may be small due to the low interwall shear strength, say 0.48 MPa for the interlayer shear strength of graphite,<sup>48</sup> as well as the shear stress concentration at the end of MWNT's, as shown in Fig. 3. Furthermore, if the tubes are incommensurate, the interlayer shear strength and stiffness may be much lower than that of graphite.<sup>40,41</sup> Once the interwall sliding takes place, the further loadings are only exerted on the outermost tube. So, if the applied tension and torsional moment loadings significantly exceed its critical value, the effective longitudinal Young's and shear moduli will become close to those of the outermost tube.

Another issue is that when the interwall interaction is improved by defects that bridge graphitic shells in MWNT's,

say chemical bonds created by electron and ion irradiation,<sup>49-51</sup> the interwall elastic constants  $E_m$  and  $G_m$  and shear strength may be increased significantly. For example, a small amount of defects can increase the interwall shear strength by several orders of magnitude.<sup>37</sup> For the situation, the present analytical expressions for the effective elastic moduli are still valid, but the values of the elastic constant  $E_m$  and  $G_m$  need to be determined based on the specific information of the defects. Also, due to the improved interwall

shear strength, the elastic range of MWNT's will increase significantly. These problems remain to be studied.

### ACKNOWLEDGMENT

This work was supported by NSF, Surface Engineering and Materials Design program under Grant No. CMS-0305594.

\*Author to whom correspondence should be addressed. Email address: j.li@ccny.cuny.edu

- <sup>1</sup>M. M. J. Treacy, T. W. Ebbesen, and J. M. Gibson, *Nature (London)* **381**, 678 (1996).
- <sup>2</sup>E. W. Wong, P. E. Sheehan, and C. M. Lieber, *Science* **277**, 1971 (1997).
- <sup>3</sup>J. Muster, M. Burghard, S. Roth, G. S. Duesberg, E. Hernández, and A. Rubio, *J. Vac. Sci. Technol. B* **16**, 2796 (1998).
- <sup>4</sup>O. Lourie, and H. D. Wagner, *J. Mater. Res.* **13**, 2418 (1998).
- <sup>5</sup>A. Krishnan, E. Dujardin, T. W. Ebbesen, P. N. Yianilos, and M. M. J. Treacy, *Phys. Rev. B* **58**, 14 013 (1998).
- <sup>6</sup>Z. W. Pan, S. S. Xie, L. Lu, B. H. Chang, L. F. Sun, W. Y. Zhou, G. Wang, and D. L. Zhang, *Appl. Phys. Lett.* **74**, 3152 (1999).
- <sup>7</sup>J. P. Salvetat, G. A. Briggs, J. M. Bonard, R. R. Bacsa, A. J. Kulik, T. Stöckli, N. A. Burnham, and L. Forró, *Phys. Rev. Lett.* **82**, 944 (1999).
- <sup>8</sup>T. W. Tomblor, C. Zhou, J. Kong, H. Dai, L. Liu, C. S. Jayanthi, M. Tang, and S. Y. Wu, *Nature (London)* **405**, 769 (2000).
- <sup>9</sup>M.-F. Yu, O. Lourie, M. J. Dyer, K. Moloni, T. F. Kelly, and R. S. Rouff, *Science* **287**, 637 (2000).
- <sup>10</sup>D. H. Robertson, D. W. Brenner, and J. W. Mintmire, *Phys. Rev. B* **45**, 12 592 (1992).
- <sup>11</sup>G. Overney, W. Zhong, and D. Tomanek, *Z. Phys. D: At., Mol. Clusters* **27**, 93 (1993).
- <sup>12</sup>B. I. Yakobson, C. J. Brabec, and J. Bernholc, *Phys. Rev. Lett.* **76**, 2511 (1996).
- <sup>13</sup>C. F. Cornwell, and L. T. Wille, *Solid State Commun.* **101**, 555 (1997).
- <sup>14</sup>J. P. Lu, *Phys. Rev. Lett.* **79**, 1297 (1997).
- <sup>15</sup>T. Halicioglu, *Thin Solid Films* **312**, 11 (1998).
- <sup>16</sup>Y. I. Prylutskyy, S. S. Durov, O. V. Ogloblya, E. V. Buzaneva, and P. Scharff, *Comput. Mater. Sci.* **17**, 352 (2000).
- <sup>17</sup>V. N. Popov, V. E. Van Doren, and M. Balkanski, *Phys. Rev. B* **59**, 8355 (1999).
- <sup>18</sup>P. Zhang, Y. Huang, P. H. Geubelle, P. A. Klein, and K. C. Hwang, *Int. J. Solids Struct.* **39**, 3893 (2002).
- <sup>19</sup>T. Chang, and H. Gao, *J. Mech. Phys. Solids* **51**, 1059 (2003).
- <sup>20</sup>Y. Jin, and F. G. Yuan, *Compos. Sci. Technol.* **63**, 1507 (2003).
- <sup>21</sup>L. Shen and J. Li, *Phys. Rev. B* **69**, 045414 (2004).
- <sup>22</sup>J. M. Molina, S. S. Savinsky, and N. V. Khokhriakov, *J. Chem. Phys.* **104**, 4652 (1996).
- <sup>23</sup>E. Hernández, C. Goze, P. Bernier, and A. Rubio, *Phys. Rev. Lett.* **80**, 4502 (1998).
- <sup>24</sup>E. Hernández, C. Goze, P. Bernier, and A. Rubio, *Appl. Phys. A: Mater. Sci. Process.* **68**, 287 (1999).
- <sup>25</sup>C. Goze, L. Vaccarini, L. Henrard, P. Bernier, E. Hernandez, and A. Rubio, *Synth. Met.* **103**, 2500 (1999).
- <sup>26</sup>L. Vaccarini, C. Goze, L. Henrard, E. Hernandez, P. Bernier, and A. Rubio, *Carbon* **38**, 1681 (2000).
- <sup>27</sup>D. Sánchez-Portal, E. Artacho, J. M. Soler, A. Rubio, and P. Ordejon, *Phys. Rev. B* **59**, 12 678 (1999).
- <sup>28</sup>G. Van Lier, C. Van Alsenoy, V. Van Doren, and P. Geerlings, *Chem. Phys. Lett.* **326**, 181 (2000).
- <sup>29</sup>G. Zhou, W. Duan, B. Gu, *Chem. Phys. Lett.* **333**, 344 (2001).
- <sup>30</sup>C. Q. Ru, *Phys. Rev. B* **62**, 9973 (2000).
- <sup>31</sup>C. Q. Ru, *Phys. Rev. B* **62**, 10 405 (2000).
- <sup>32</sup>J. Z. Liu, Q. Zheng, and Q. Jiang, *Phys. Rev. Lett.* **86**, 4843 (2001).
- <sup>33</sup>G. M. Odegard, T. S. Gates, L. M. Nicholson, and K. E. Wise, NASA Technical Report, NASA/TM-2001-210863 (2001) (unpublished).
- <sup>34</sup>C. Li, and T.-W. Zhou, *Int. J. Solids Struct.* **40**, 2487 (2003).
- <sup>35</sup>C. Li, and T.-W. Zhou, *Compos. Sci. Technol.* **63**, 1517 (2003).
- <sup>36</sup>S. Iijima, C. Brabec, A. Maiti, and J. Bernholc, *J. Chem. Phys.* **104**, 2089 (1996).
- <sup>37</sup>M. Huhtala, A. V. Krascheninnikov, J. Aittoniemi, S. J. Stuart, K. Nordlund, and K. Kaski, *Phys. Rev. B* **70**, 045404 (2004).
- <sup>38</sup>C. Q. Ru, *J. Appl. Phys.* **87**, 7227 (2000).
- <sup>39</sup>J. E. Lennard-Jones, *Proc. R. Soc. London* **A106**, 441 (1924).
- <sup>40</sup>G. He, M. H. Müser, and M. O. Robbins, *Science* **284**, 1650 (1999).
- <sup>41</sup>M. H. Müser, and M. O. Robbins, *Phys. Rev. B* **61**, 2335 (2000).
- <sup>42</sup>A. N. Kolmogorov and V. H. Crespi, *Phys. Rev. Lett.* **85**, 4727 (2000).
- <sup>43</sup>W. Guo, Y. Guo, H. Gao, Q.-S. Zheng, and W. Zhong, *Phys. Rev. Lett.* **91**, 125501 (2003).
- <sup>44</sup>W. N. Reynolds, *Physical Properties of Graphite* (Elsevier, New York, 1968).
- <sup>45</sup>R. Martel, T. Schmidt, H. R. Shea, T. Hertel, and Ph. Avouris, *Appl. Phys. Lett.* **73**, 2447 (1998).
- <sup>46</sup>C.-J. Park, Y.-H. Kim, and K. J. Chang, *Phys. Rev. B* **60**, 10 656 (1999).
- <sup>47</sup>M.-F. Yu, T. Kowalewski, and R. S. Rouff, *Phys. Rev. Lett.* **86**, 87 (2001).
- <sup>48</sup>D. E. Soule and C. W. Nezbeda, *J. Appl. Phys.* **39**, 5122 (1968).
- <sup>49</sup>F. Banhart, *Rep. Prog. Phys.* **62**, 1181 (1999).
- <sup>50</sup>H. Stahl, J. Appenzeller, R. Martel, P. Avouris, and B. Lengeler, *Phys. Rev. Lett.* **85**, 5186 (2000).
- <sup>51</sup>A. V. Krascheninnikov, K. Nordlund, and J. Keinonen, *Appl. Phys. Lett.* **81**, 1101 (2002).